Pin-Joint Design Effect on the Reliability of a Polysilicon Microengine

Danelle M. Tanner, Jeremy A. Walraven, Seethambal S. Mani, and Scot E. Swanson
Sandia National Laboratories
P. O. Box 5800, M/S 1081, Albuquerque, NM 87185-1081
505-844-8973; fax: 505-844-2991; e-mail: tannerdm@sandia.gov

ABSTRACT

Accelerated stress experiments were performed on a class of pin joints to determine reliability. We varied parameters that affected the area of the rubbing surfaces and the gap between those surfaces. Most of the pin joints failed due to seizure. We observed bimodal failure distributions where the lower distribution was associated with an adhesion event with no observable wear debris. The upper distribution of failures was associated with agglomerations of wear debris, which may have seized the pin joint. The effect of surface coatings was also studied. We found that for supercritical carbon dioxide ($SCCO_2$) dried microengines; the largest effect was due to gap spacing. For microengines with a self-assembled monolayer coating (SAMS), we observed minimal difference in the lifetimes of failed devices. [*Keywords:* MicroElectroMechanical System, MEMS Reliability, and MEMS Wear]

INTRODUCTION

Reliability studies and predictions are becoming crucial to the success of MicroElectroMechanical System (MEMS) as commercial applications are developed. For many MEMS devices, especially actuators, normal operation requires surfaces to come into contact and rub against one another. In these cases wear of the rubbing surfaces becomes a critical reliability issue. One of the first experiments [1] to show wear as a dominant failure mechanism ran polysilicon microturbines [2] and gears at rotational speeds up to 600,000 rpm. A focused air jet directed at the turbine induced the rotation. Gabriel et al. [1] estimated dynamic coefficients of friction between polysilicon and silicon ranging in value from 0.25 to 0.35. The wear was extensive enough to cause misalignment followed by wedging of the device.

Previous experiments [3] on the lifetime of a surface-micromachined microengine revealed wear as the dominant failure mechanism. The median cycles to failure ranged from 10^5 to 10^6 with several microengines reaching close to 10^9. A predictive reliability model for the microengine was developed which was based on the fundamental physics of wear in a mechanically resonating system. In another study of the microengine, it was determined that the introduction of an additional source of rubbing surfaces (in this case, a dimple rubbing against a shuttle) reduced the lifetime and thus, the reliability of the microengine [4].

The study presented in this work used the electrostatically driven microactuator (microengine) developed at Sandia National Laboratories [5]. The microengine consists of orthogonal linear comb drive actuators mechanically connected through the shuttle and linkage arms to a rotating gear as seen in Figure 1. By use of an offset pin joint, the linear displacement of the comb drives was transformed into the circular motion of the gear. The gear rotates about a hub, which is anchored to the substrate.

The pin joint of a surface-micromachined microengine is the most crucial component for reliable operation. Past work has shown that

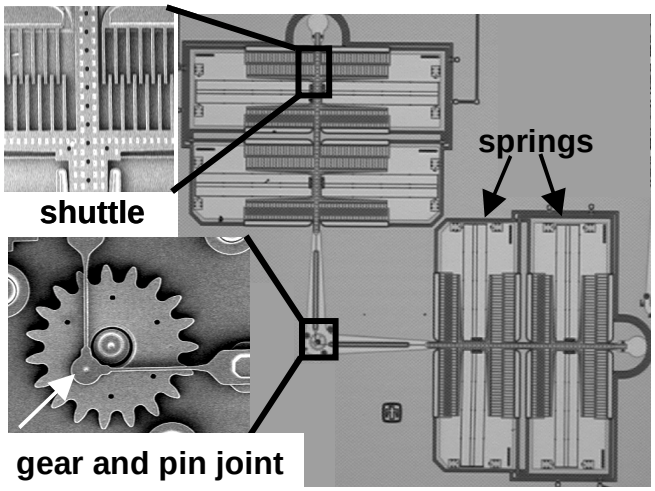

Figure 1. This SEM image of the fabricated microengine shows the orthogonal-positioned, electrostatic actuators, which provide linear motion. The shuttle and comb fingers are shown in the upper inset. The lower inset shows an enlarged view of the output gear and the location of the pin joint.

wear and adhesion in the pin joint are the dominant failure mechanisms in microengines [6, 7]. It has been shown that changing the material of the rubbing surfaces, to tungsten-coated polysilicon, for example, increased the lifetime by 3 orders of magnitude [8]. However, in this study, we used polysilicon pin joints in order to study the design effect more readily. The parameters modified were contact area of the interacting surfaces and gap spacing between the surfaces. The pin joint and hub of the output gear use a similar fabrication process, thus the hub was changed also.

The objective of this work is to determine the pin-joint design that yields the most reliable performance.

PIN-JOINT DESIGNS

The fabrication of a pin joint provides a rotational degree of freedom in the Sandia SUMMiT™ process, which builds micromachines by using alternating depositions (layers) of polysilicon and sacrificial silicon dioxide. It is achieved through several process steps, as shown in Figure 2. Three pin-joint designs were studied; they are labeled designs A, B, and C.

The pin joint fabrication steps for design A start with a poly1 cut exposing the underlying oxide. A timed wet etch using hydrofluoric acid (HF) based chemistry produces a hollowed out region in the oxide. A conformal oxide (0.5 or 0.3 μm-thick) is then deposited providing a gap between the pin joint and surrounding poly surfaces. In the final step, the deposition of the conformal poly2 layer, the hollowed out region is filled forming the pin joint. During the release process, all of the oxide material is etched away leaving a freely rotating pin supported by the poly1 layer.

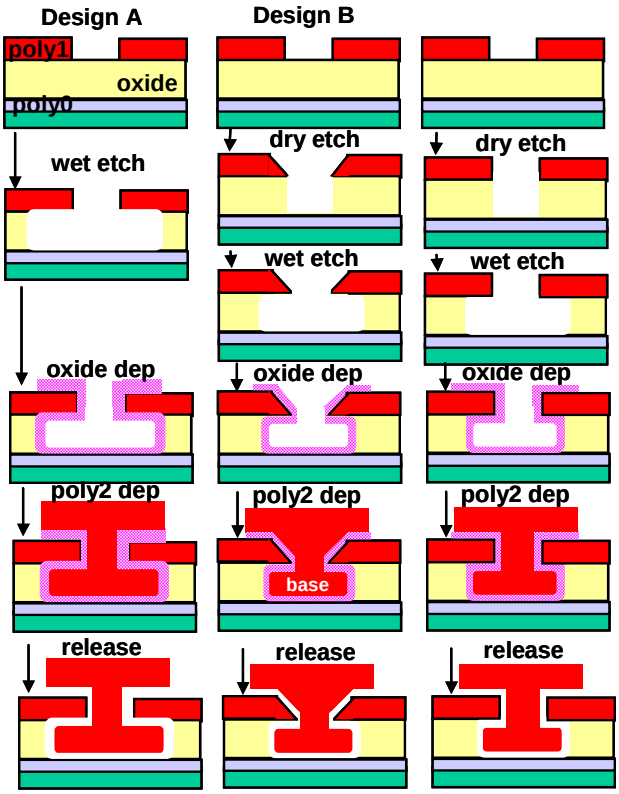

Figure 2. The process steps to fabricate a pin joint in the three designs are shown above. After the wet-etch step, all designs go through an oxide deposition (split between 0.3 and 0.5 µm) and a poly2 deposition to form the pin joint.

The process steps for design B are similar, except that the wet etch has been replaced by a combination of dry etch and wet etch. The dry etch affects the side wall profile of the poly1 as shown in Figure 2. Note that a shorter wet etch in this design produced a smaller base of the pin joint, decreasing the area of interacting surfaces. Identical steps to design A, a conformal oxide (0.5 or 0.3 µm-thick) and poly2 deposition, were then followed.

In design C, the dry etch process was modified to obtain a more vertical sidewall profile in poly1. Identical steps to design A and B, a conformal oxide (0.5 or 0.3 µm-thick) and poly2 deposition, were then followed.

In both design B and C, the gap spacing (defined by the oxide deposition thickness) was varied. We wanted to determine if reducing the tolerance in the gaps would prevent wobble and perhaps increase functionality.

Figure 3 shows an as-fabricated comparison of the three designs. These cross sections were formed using a Focused Ion Beam (FIB) to cut through the polysilicon layers. The diameter of the pin joint is nominally 3 µm. The width of the lower base of the pin joint in design B is smaller, which was intended to minimize surface contact area and thus reduce wear. The other major difference in design B is the poly1 cut profile (see arrows in Figure 3) yielding an angled pin joint diameter. Design C was an attempt to produce a poly 1 cut profile more like that of design A, but was not optimized yielding a slight profile in the poly1 cut. In all the designs, the poly3 layer provided the connection to the linkage arms.

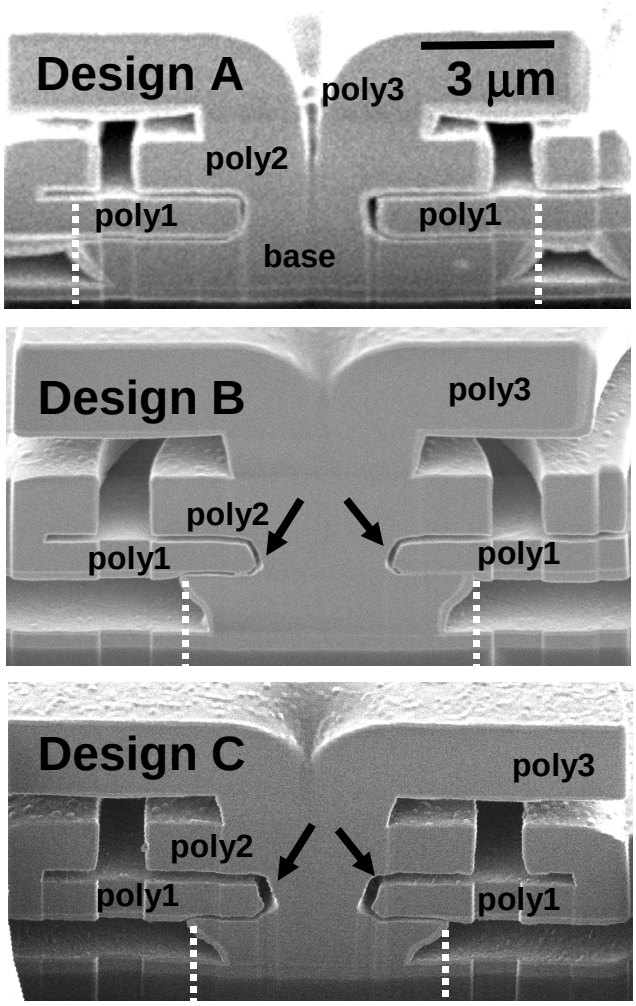

Figure 3. This FIB cross-section of the pin joint area shows the 'as-fabricated' designs on the same scale. Design B has an altered poly1 cut profile (arrows) and the base has a smaller width (decreased area of interacting surfaces) as indicated by the dashed lines. We expected design C to have a straight poly1 cut profile, but it is also slightly altered.

Experimental Procedure

Sample Preparation

Surface micromachined MEMS are mechanical structures fabricated from deposited thin films. The structures are encased in sacrificial layers (typically SiO_2) until ready for use. The oxide film is etched by hydrofluoric acid (HF) to yield a "released" sample. There are several strong adhesive forces that act on the structures during the drying stage of the release [9]. These include capillary, electrostatic, and van der Waals. Capillary forces dominate at these dimensions and processes have been developed to reduce or eliminate these forces for successful operation of the MEMS structure [10]. For example, coupling agent coatings such as alkysilanes have been used to increase the hydrophobicity of the polysilicon surface.

The most studied silane coatings deposited on silicon are octadecyltrichlorosilane (OTS) precursor molecules having a chemical formula of $C_{18}H_{37}SiCl_3$. Additionally, a fluorinated chain, perfluorodecyltri-

chlorosilane (FTS, $C_6F_{13}CH_2SiCl_3$), has been studied by Alley et al. [11]. Application of a coupling agent requires preparation of the polysilicon surface by an oxidation step (H_2O_2), resulting in an oxide layer a few nanometers thick.

An alternate approach to applying a coupling agent is to prevent the formation of a meniscus by eliminating the liquid phase in the drying process. This method is supercritical CO_2 drying [12] and it has been successfully applied to surface micromachining.

In these experiments we used samples that had either an FTS surface treatment or samples that were supercritical carbon dioxide dried ($SCCO_2$). The $SCCO_2$ samples had no specific oxidation step, but were in an air environment that would promote growth of a native oxide.

Microengine Lifetime Experiment

Model-based drive signals for microengines were derived previously [13] and a software code [14] was developed to provide the properly timed voltage signals to the actuators. The code provides an interface to set various parameters in the drive signals. Two of these parameters are radial force and longitudinal force that the actuators provide to the pin joint. We typically set the radial force to zero and the microengine will operate with a longitudinal force as low as 1 μN.

As seen in Figure 4, under an operating condition of 500 Hz or less the majority of microengines with symmetric actuators will rotate for roughly 10^9 cycles before failure due to wear/adhesion in the pin joint [15]. However, at higher frequencies (we have tested up to 3000 Hz) this number of cycles to failure is reduced by 3 to 4 orders of magnitude implying that frequency is a failure-acceleration parameter.

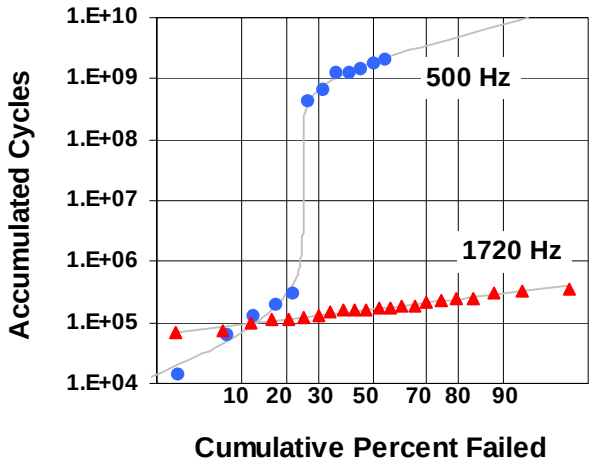

Figure 4. This graph shows the difference in accumulated cycles to failure for a low frequency of 500 Hz and the higher frequency of 1720 Hz.

We suspect that this effect was due to additional force exerted on the pin joint at the higher frequencies. Figure 5 shows the linkage arms of a gearless microengine and the 17-μm-radius circle that the linkage arms should follow for proper operation. We have developed strobe and imaging techniques [16] and observed proper circular motion for frequencies below 500 Hz. However, at higher frequencies, the circular motion was elongated into an oval (Figure 5) indicating that some additional force was present. This additional force

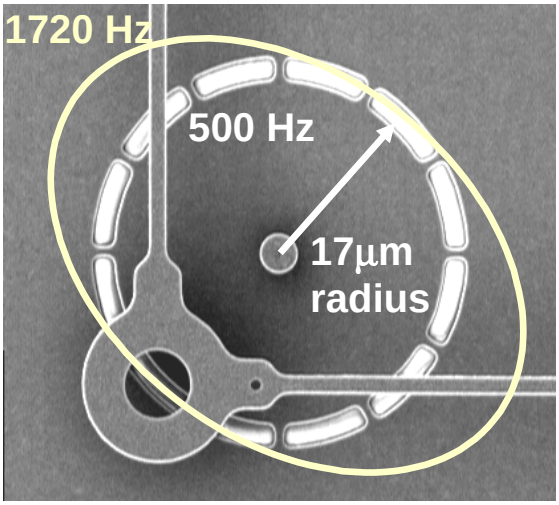

Figure 5. The path of a gearless microengine is shown for two frequencies. The 500 Hz path followed the dashed circle of 17-μm radius. The elongated path at 1720 Hz was due to additional forces, most likely because of an absence of the proper dynamic terms in the model.

is most likely due to an absence of the proper dynamic terms in the model.

We used two different microengines in this experiment. The microengines with pin-joint design A were fabricated using a process producing a ground plane and three mechanical layers of polysilicon. The restoring springs in this actuator are doubly stacked with a measured spring constant of 0.083 N/m. The spring-constant measuring technique is described in [17]. The microengines with pin-joint designs B and C were fabricated using a process producing a ground plane and four mechanical layers of polysilicon. The restoring springs in this actuator are triple stacked with a measured spring constant of 0.145 N/m. The microengine resonant frequency for design A was 1200 Hz and for designs B and C was 1300 Hz. These resonant frequencies are similar; therefore, we expect no differences in the lifetime results from the frequency acceleration.

We performed the experiments in a laboratory environment where the humidity ranges from 30% to 50% RH and the temperature ranges from 21 to 23 degrees C. In this humidity range, the amount of wear debris generated is typically minimized due to a lubrication mechanism associated with adsorbed water vapor [18]. The microengines were not packaged, but were on ¼ wafer pieces. We chose a drive frequency of 1720 Hz and a longitudinal-load force of 5.0 μN. Both of these conditions of frequency and force accelerated the time to failure. In each experiment, the microengines were stressed until failure and failure was defined as the inability of the drive gear to make a full rotation.

RESULTS AND DISCUSSION

Most experiments had a reasonable failure distribution using 20 samples, but we observed two bimodal distributions that required more samples to zero in on the median number of cycles to failure of the majority. Figure 6 shows examples of distributions from the three designs and the corresponding fits to the data. All had a gap spacing of 0.5 μm and were $SCCO_2$ dried. Each lognormal distribution can be described by the median number of cycles to failure and a slope parameter, σ. The median number of cycles to failure is simply the intersection of the data fit line and the 50% cumulative failed. The slope parameter is the slope of the fit line on a log scale.

The data distributions show the variation of accumulated cycles to failure of similar microengines. The design A data yielded the only unimodal distribution. It had a median number of cycles to failure of 3.4 x 10^5 with a slope parameter, σ, of 0.25. The data for design B exhibited a bimodal distribution where 34 failed microengines were needed to determine that the upper part of the distribution had the majority of the data. We deconvolved the bimodal distributions and used the median accumulated cycles to failure of the upper (majority) distribution in further analysis. For the case of design B, the median number of cycles to failure was 8.2 x 10^5 with a slope parameter, σ, of .33. Two outliers (low and high) were ignored in the fit to the design C data. The remaining data points were also deconvolved and the majority (upper) distributions median point was used. Design C had a median number of cycles to failure of 4.8 x 10^5 with a slope parameter, σ, of 0.26. Although Figure 6 shows a wide range for accumulated cycles to failure, the majority of each distribution is in agreement. There is virtually no difference in designs A, B, or C for a 0.5-µm-gap spacing and $SCCO_2$ dried. This implies that reducing the area of interacting surfaces by changing the base width of the pin joint had no effect on the reliability for this gap spacing. This may be telling us that the important surfaces are the sidewalls of the pin joint, not the horizontal surfaces. The largest difference in the distributions in Figure 6 lies in the early failures, up to 30% cumulative percent failed, which are normally described as the "defect" distributions. Design A had no defect distribution, which is preferred.

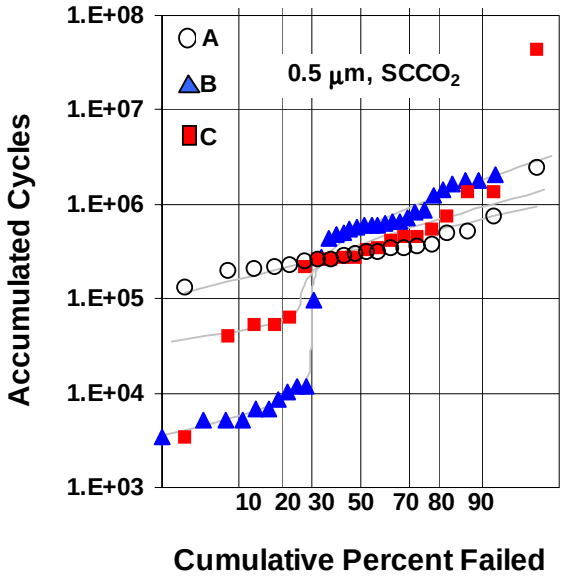

Figure 6. This plot shows data from three separate tests representing each design. The gap spacing was 0.5 µm and the microengines from these three tests were $SCCO_2$ dried.

Figure 7 shows the corresponding data from the 0.3-µm-gap spacing. Data from design A is missing because that split (0.3 µm) had a fabrication problem. The two largest data points for design B were considered outliers in the fit, which yielded a median number of cycles to failure of 3.2 x 10^4 with a slope parameter of 0.20. The data from design C was difficult to interpret because roughly 55% of the data laid in the lower section and 45% was in the high slope upper section. We repeated that experiment with another ¼ of the same wafer to sort out the analysis. The data from the repeat experiment agreed with the lower section, which prompted us to use a median number of cycles to failure of 1.3 x 10^4 for further analysis. The difference in the shape of the data from design C and the repeat test is still unclear. The high slope of the upper section might indicate a different failure mechanism. The majority of observed bimodal distributions for failed microengines have the same slope for upper and lower distributions.

Stress Experiment Summary

The results of all experiments are shown in Figure 8 where the data points represent the majority of the distribution. The median number of cycles to failure was determined from each distribution and the slope parameter was used to determine the 90% confidence limits shown as error bars in the plot.

We see from Figure 8 that there appears to be an effect due to the gap spacing. This is much more apparent in the $SCCO_2$ data, where for

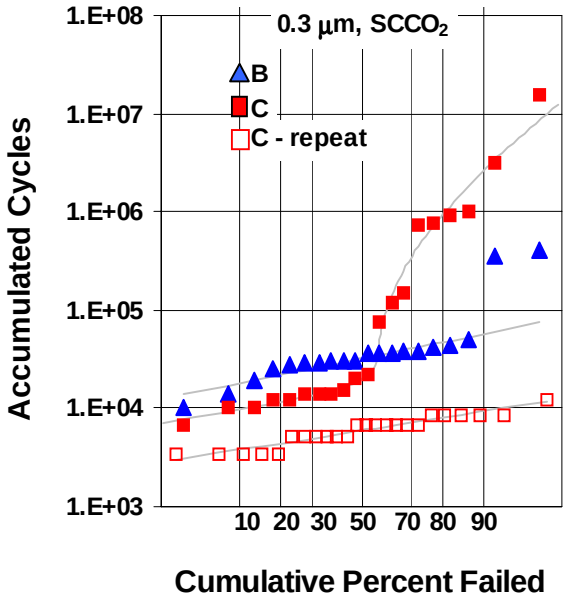

Figure 7. This plot shows data from two separate designs. The gap spacing was 0.3 µm and the microengines from these tests were $SCCO_2$ dried. Design A is missing due to a fabrication problem.

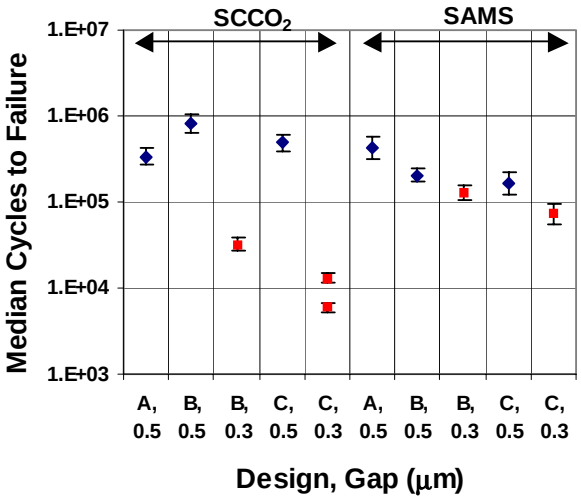

Figure 8. This data from all of the experiments shows the possible effect of gap spacing on the reliability.

design B there is a factor of 25 difference in the two median cycles to failure. In design C, the difference is greater with a factor of 37 between the median cycles to failure of the 0.5-μm gaps to the 0.3-μm gaps. For the SAMS coated microengines, the gap spacing factors are only 1.6 and 2.3 for designs B and C, respectively. This minimal difference in median cycles to failure may be due to the lubricating effect of the coating. Srinivasan et al. [19] measured a low friction coefficient for SAMS coated structures, but after repeated sliding the friction coefficient increased and sticking was observed.

Comparing design A results with design B and C (Figure 8), in order to understand the base-width parameter, yields conflicting results for the two releases. In the $SCCO_2$ case, the smaller width of design B and C has slightly longer lifetimes. However, for the SAMS coated case, Design A has a slightly longer lifetime than designs B and C. Because the differences in the distributions are so slight, the results probably indicate that the base width parameter is not a factor.

The SAMS coated microengines for the larger gap size have slightly shorter lifetimes than the comparable $SCCO_2$ dried microengines. This indicates that although the SAMS coating may be initially lubricating, it is not wear resistant.

In work done previously [6] we found that our microengines failures at frequency fit an adhesive wear model. Bimodal distributions, as observed in this work, may be explained as follows. Adhesive wear occurs when the asperities between two surfaces form an adhesive bond. In the case of polysilicon, if the passivating oxide layer is worn away and two areas of polysilicon touch, the dangling bonds on the surfaces can cause adhesion. If the surface area is large enough, this could seize the microengine. However, if the surface area is smaller, the asperity could simply tear away, leaving a particle transferred to one surface or freed to become debris. In this way, material can transfer from one surface to another or create wear debris, and result in regions where the microengine can begin to stick and seize, as observed.

The next section on failure analysis systematically goes through a representative failure for each distribution and using a FIB, observes the pin-joint region. The objective was to investigate any wear and look for trends.

Failure Analysis

Failure analysis of these microengines was initially performed using optical microscopy. All failures of design B and C were observed as seized drive gears. There were two failures in SAMS-coated design A where the pin joint broke away from the gear. Both of these failures had a high number of accumulated cycles. This failure has been observed before [6] and the typical cause was thinning of the pin joint due to excessive wear.

$SCCO_2$ Dried Microengines: A design A microengine that was $SCCO_2$ dried and failed at 2.5×10^6 cycles was investigated by a FIB cut through the pin joint area. Results of that cut are shown in Figure 9. Debris is observed accumulating along the exposed poly1 gear surface and the edge of the pin joint. These results are consistent with what had been observed in previous wear experiments [3, 6].

Results obtained from microengine pin joints fabricated with design B with 0.5-μm gap spacing and $SCCO_2$ drying have a bimodal failure distribution (Figure 6). As shown in Figure 10, the pin joints have failures at 6.9×10^3 and 1.8×10^6 cycles to failure respectively. The first sample (6.9×10^3) shows no signs of wear. FIB analysis of the pin joint of this microengine did not reveal the adhered site leading to failure. After FIB processing, the sample is still in the stuck position indicating we have not reached the failure site. Further FIB analysis may reveal the failure site or free up the device, compromising the failure mechanism. In the microengine operated for 1.8×10^6 cycles, wear debris is observed along the pin joint and gear regions. Closer observation of the gear that contacts the pin joint shows rounding of that area. That geometry is different from the as-fabricated geometry indicating that material is being worn off from that region of the gear. Optical inspection did not reveal any wear debris along the top surface of the gear or ground plane indicating the debris was self-contained along the pin joint. In this case, the failure could be due to an adhesion event or the accumulation of wear debris.

FIB characterization of design B microengine pin joints with 0.3 μm gap spacing and $SCCO_2$ drying do not show as much wear debris as their 0.5 μm counterparts. This sample was operated for 3.6×10^4 cycles before seizing. When compared to a control sample shown in Figure 11, the adhesion area is observed along the gear/pin joint area (arrow). The lack of wear debris was probably due to the occurrence of an adhesion event between the pin joint and the gear. This adhesion seized the pin joint and prevented further wear. Adhesion is the first step to adhesive wear.

In microengines fabricated with design C and $SCCO_2$ dried, analysis of the pin joint of a microengine that failed after 4.5×10^5 cycles, did

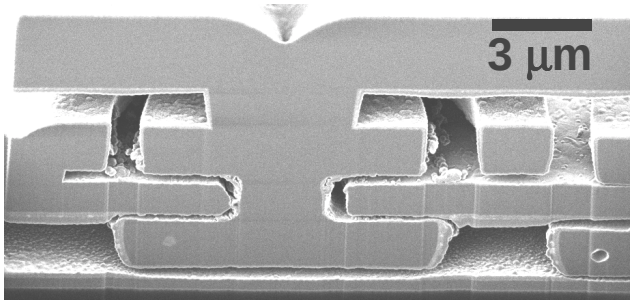

Figure 9. This FIB cut in a design A microengine that was $SCCO_2$ dried and stressed to 2.5×10^6 cycles shows wear debris accumulation in the rubbing surface area of the pin joint.

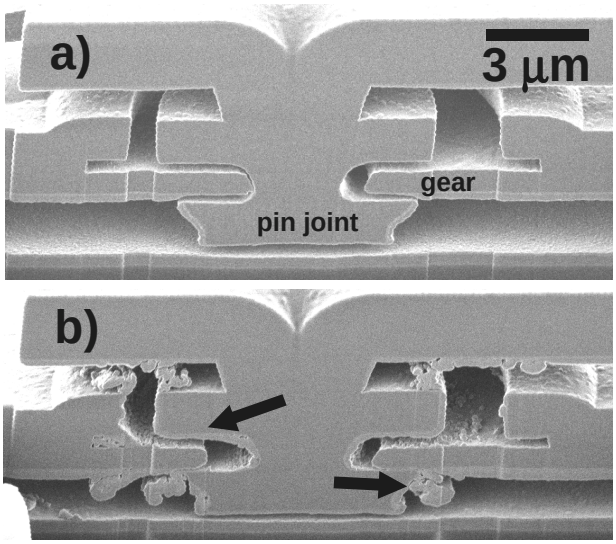

Figure 10. FIB cross-sections of $SCCO_2$ dried, design B pin joints in microengines with a 0.5-μm-gap spacing after **a)** 6.9×10^3 cycles and **b)** 1.8×10^6 cycles. The microengine in a) likely failed from an adhesion event causing it to seize.

not reveal much wear debris along this region, as seen in Figure 12. These results are consistent with what was observed in design A microengines tested at similar humidity levels [6]. A pin joint of a microengine operated to 4.4 x 10^7 cycles shows more signs of wear along the pin joint region. Debris is observed accumulating along the exposed poly1 gear surface and the edge of the pin joint. Again, these results are consistent with what had been observed in previous experiments [3, 6]. FIB cross sections also revealed a misalignment between the top poly surface and the pin joint. At this point, we do not believe this will significantly affect our results of wear along rubbing surfaces contained within the pin joint.

Examination of microengine pin joints processed in design C with a 0.3 μm gap spacing and $SCCO_2$ drying again reveals failure through wear of rubbing surfaces. One microengine failed after 2.1 x 10^4 cycles shows very little wear debris contained within the pin joint. The failure mechanism in this microengine appears to be adhesion between the pin joint and the gear. In another microengine, wear debris has accumulated within the pin joint region. In these pin joint designs the gap spacing is tighter to reduce wobble, but it confines the space where smaller amounts of wear material can cause a microengine to seize after operation at fewer cycles. As shown in Figure 13, the adhesion sites and worn material have been identified (arrow). Failures with small amounts of wear debris are again consistent with previous findings, and may be more impacted by the smaller gap spacing.

SAMS Coated Microengines: Microengines processed with a lubricating SAMS coating were also analyzed after testing. Failure analysis of microengines fabricated with design B with a 0.5 μm gap spacing reveal debris in the pin joint area similar to it's $SCCO_2$ released counterpart. Very little wear debris is observed in the pin joint after 1.9 x 10^4 cycles, as seen in Figure 14. Contact is observed along the gear/ pin joint sidewall. The microengine operated up to 3 x 10^5 cycles shows signs of wear and degradation along the pin joint and gear areas. The debris has accumulated along the sidewall region of the pin joint as well as the lower portions of the pin joint and gear respectively.

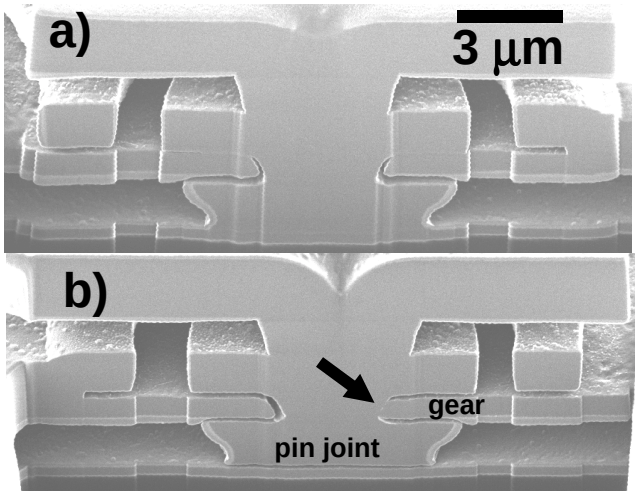

Figure 11. FIB cross-sections of $SCCO_2$ dried, design B pin joints in microengines with a 0.3-μm-gap spacing. **a)** control sample, **b)** pin joint after 3.6 x 10^4 cycles. The arrow shows the failure site, which is a region of adhesion between the pin joint and the gear.

SAMS coated microengines from design B with a 0.3-μm-gap spacing were also investigated. Figure 15 shows the FIB cross section of a pin joint stressed to 1.8x 10^5 cycles. There is wear debris accumulating at the pin joint gear interface as well as in the outer regions. There was a large chunk (arrow) between the gear surface and the linkages arms, which was not characteristic with earlier observations.

FIB cross sections were performed on microengine pin joints from the other SAMS experiments using design A and design C. The

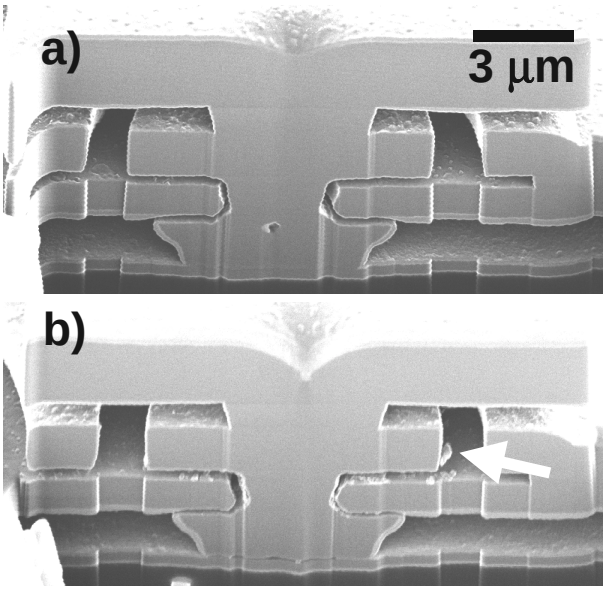

Figure 12. FIB cross-sections of $SCCO_2$ dried, design C pin joints in microengines with a 0.5-μm-gap spacing after **a)** 4.5 x 10^5 cycles and **b)** 4.4 x 10^7 cycles. Wear debris is observed along the gear and outer region of the pin joint (arrow). Both microengines failed from wear of rubbing surfaces causing the

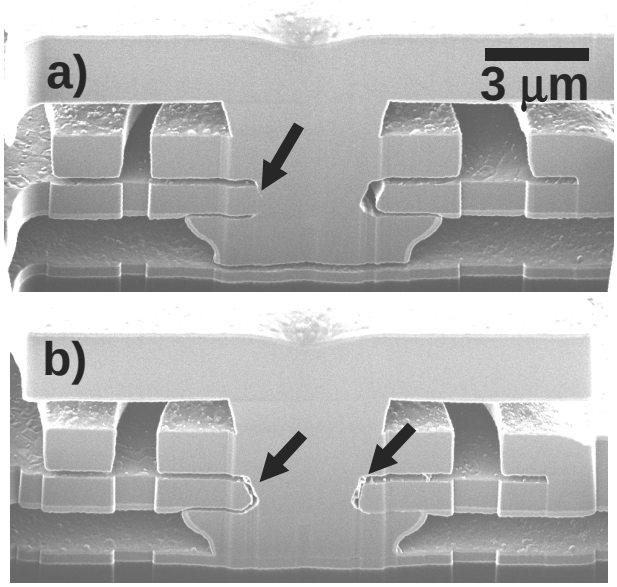

Figure 13. FIB cross-sections of $SCCO_2$ dried, design C pin joints in microengines with 0.3-μm-gap spacing after **a)** 2.1 x 10^4 cycles and **b)** 9.3 x 10^5 cycles. Note the adhesion between the gear and pin joint in **a)**, and the wear debris contained in the small gap of **b)**. Both microengines failed from wear of rubbing surfaces causing the microengines to seize.

results agree with what has been presented here so no further figures were required.

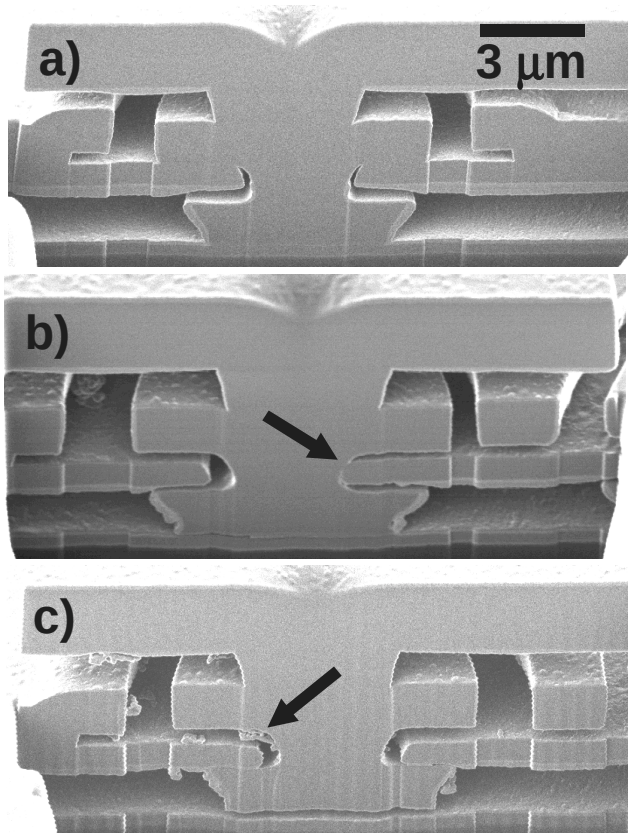

Figure 14. FIB cross-sections of SAMS coated, design B pin joints in microengines with a 0.5-μm-gap spacing. **a)** control, **b)** 1.9 x 10^4 cycles, and **c)** 3 x 10^5 cycles. There may be an adhesion in b) near the arrow. Wear debris is observed along the gear and outer region of the pin joint of the microengines in c). The arrow shows the accumulation.

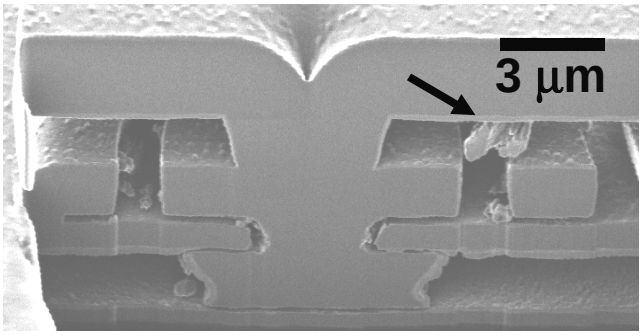

Figure 15. FIB cross-section of SAMS coated, design B pin joints in microengines with a 0.3-μm-gap spacing that failed at 1.8 x 10^5 cycles. Wear debris is observed along the gear and outer region of the pin joint (arrow).

Failure Analysis Summary: We have observed accumulation of wear debris only after roughly 10^5 cycles. In most cases of lower cycles, the microengines are seized, probably due to an adhesion event. We observed three of these in the four FIB cuts at low failure cycle. At the higher number of cycles to failure, we typically observe accumulation of wear debris. In these cases, it is not clear if the failure is due to that accumulation or due to an adhesion event.

Wear Discussion

Bimodal Distributions: For the case of our bimodal distributions, we observed no wear debris for the lower distributions and in many cases observed the adhesion area. This adhesion is representative of the first step in adhesive wear. In many cases, the force of the microengine linkage arms could break the initial adhesion and continue operating. A continuation of this process resulted in the upper distributions of failure where we observed large amounts of wear debris. The wear debris formation introduced three-body wear, probably including abrasive wear, which lead to more wear debris. The dramatic influence of third body wear upon tribological processes is well known [20]. We are not certain if the upper distribution failures are due to an adhesion event or an accumulation of wear debris.

Gap Size: Wear in a confined space such as the gap in a pin joint is a very complex problem. The majority of works on the formation and the role of wear debris/particles have been performed on "open" sliding systems. In these tests, the wear particles are not trapped. Unfortunately, in our microengine, the wear particles were trapped and agglomerated into larger debris, roughly 200 nm in diameter. Rabinowicz [21] shows that the seizure of close-toleranced sliding components arises whenever the clearance is smaller that the largest wear particles produced by the sliding system. However, the real culprit is agglomeration of particles. Mosleh et al. [22] found that agglomeration of wear particles in bearings increased the normal load at the contact point, leading to seizure. In this experiment, the differences were a factor of 25 and 37 in the median number of cycles to failure between the 0.5-μm gap and the 0.3-μm gap. Clearly, a gap size of 0.3 μm was too small for the uncoated, $SCCO_2$ dried microengines leading to early seizure.

CONCLUSIONS

We have observed a dependence of the lifetime of a microengine on the pin joint design, but it is only prominent in $SCCO_2$ dried devices. The most important parameter was gap spacing, where the larger gap produced longer lifetimes. The lack of a more pronounced difference in the SAMS coated parts may be due to the lubricating effect of the coating. However, in comparing the lifetimes of SCCO coated parts to SAMS coated microengines we observe no improvement in lifetime indicating that the SAMS coating is not wear resistant.

The base width of the pin joint had only a minimal effect on the lifetimes of the microengines, which may indicate that the important sliding surfaces are the vertical sidewalls of the pin joint and poly1 gear. This sidewall surface was where all adhesion regions were observed.

The bimodal distributions were representative of a normal progression of adhesive wear. The early adhesion events in which no wear debris was observed could be the first stage of the process. The later seizures in which wear debris was observed was characteristic of a three-body wear process.

These results illustrate the need to explain effects of design on reliability and lifetimes. There is always a tradeoff – in this case the larger gap allowed more wobble, but a smaller gap caused early seizures. As Rabinowicz [23] stated for macro systems,

> "Many engineers have found that in practice, when they take a successful mechanical device and try to improve its

performance by reducing the clearances of the sliding members, a condition results at which the device no longer functions but rather seizes very quickly after being placed into operation."

This statement holds true for microsystems where we have shown that the gap spacing is a critical parameter for reliability.

ACKNOWLEDGMENTS

The authors thank the personnel of the Microelectronics Development Laboratory at SNL for fabricating and releasing the devices used in this experiment. We also thank Alex Pimentel and Teresa Gutierrez for providing the FIB work paramount to evaluating the pin joints. Sandia is a multiprogram laboratory operated by Sandia Corporation, a Lockheed Martin Company, for the United States Department of Energy under contract DE-AC04-94-AL85000.

REFERENCES

[1] K. J. Gabriel, F. Behi, and R. Mahadevan, "In situ Friction and Wear Measurements in Integrated Polysilicon Mechanisms," *Sensors and Actuators*, **A21-A23**, 1990, pp. 184-188.

[2] M. Mehregany, K. J. Gabriel, and W. S. N. Trimmer, "Integrated fabrication of polysilicon mechanisms," *IEEE Trans. Electron Devices*, **ED-35**, 1999, pp. 719-723.

[3] D. M. Tanner, W. M. Miller, W. P. Eaton, L. W. Irwin, K. A. Peterson, M. T. Dugger, D. C. Senft, N. F. Smith, P. Tangyunyong, and S. L. Miller, "The Effect of Frequency on the Lifetime of a Surface Micromachined Microengine Driving a Load," *IEEE International Reliability Physics Symposium*, Reno, NV, 1998, pp. 26-35.

[4] D. M. Tanner, K. A. Peterson, L. W. Irwin, P. Tangyunyong, W. M. Miller, W. P. Eaton, N. F. Smith, M. S. Rodgers, "Linkage Design Effect on the Reliability of Surface Micromachined Microengines Driving a Load," *Proceedings of SPIE*, **Vol. 3512**, pp. 215-226.

[5] E. J. Garcia and J. J. Sniegowski, "Surface micromachined microengine," Sensors and Actuators A, **Vol. 48**, 1995, pp. 203-214.

[6] D. M. Tanner, W. M. Miller, K. A. Peterson, M. T. Dugger, W. P. Eaton, L. W. Irwin, D. C. Senft, N. F. Smith, P. Tangyunyong, and S. L. Miller, "Frequency Dependence of the Lifetime of a Surface Micromachined Microengine Driving a Load," in *Microelectronics Reliability Journal*, **39** (1999) pp. 401-414.

[7] J. A. Walraven, T. J. Headley, A. N. Campbell and D. M. Tanner, "Failure Analysis of Worn Surface Micromachined Microengines," in *Proceedings of SPIE* , **Vol. 3880**, 1999, pp. 30-39.

[8] S. S. Mani, J. G. Fleming, J. A. Walraven, J. J. Sniegowski, M P. de Boer, L. W. Irwin, D. M. Tanner, D. A. LaVan, M. T. Dugger, J. Jakubczak, and W. M. Miller, "Effect of W Coating on Microengine Performance," *Proceedings of IRPS*, 2000, pp.146-151.

[9] R. Maboudian and R. T. Howe, "Critical Review: Adhesion in surface micromechanic structures," *Journal Vac. Sci. Technol.*, **B 15(1)**, Jan/Feb 1997, pp. 1-20.

[10] R. Maboudian and R. T. Howe, "Stiction reduction processes for surface micromachines," *Tribology Letters*, **3**, 1997, pp. 215-221.

[11] R. L. Alley, R. T. Howe, and K. Komvopoulos, "The effect of release-etch processing on surface microstructure stiction," *Proceedings of the IEEE Solid-State Sensor and Actuator Workshop*, Hilton Head, SC, 1992, pp. 202-207.

[12] C. J. Kim, J. Y. Kim, and B. Sridharan, "Comparative evaluation of drying techniques for surface micromachining," *Sensors and Actuators*, **A64**, 1998, pp. 17-26.

[13] S. L. Miller, J. J. Sniegowski, G. LaVigne, and P. J. McWhorter, "Performance tradeoffs for a surface micromachined microengine," *Proceedings of SPIE Micromachined Devices and Components II*, **Vol. 2882**, Austin, October. 14-15, 1996, pp. 182-191.

[14] N. F. Smith, D. M. Tanner, G. F. LaVigne, S. L. Miller, W. P. Eaton, L. W. Irwin, "Super μDriver V1.0," copyright, 1998.

[15] D. M. Tanner et al., "MEMS Reliability: Infrastructure, Test Structures, Experiments, and Failure Modes," *Sandia Report*, SAND2000-0091, January, 2000, pp. 155-157. Download from http://www.prod.sandia.gov/cgi-bin/techlib/access-control.pl/2000/000091.pdf

[16] W. P. Eaton, N. F. Smith, L. Irwin, D. M. Tanner, J. J. Allen, S. L. Miller, and W. M. Miller, "Characterization Techniques for Surface-Micromachined Microengines," *SPIE's 1998 Symposium on Micromachining and Microfabrication*, Santa Clara, CA, **Vol. 3514**, pp. 171-178.

[17] N. F. Smith, W. P. Eaton, D. M. Tanner, and J. J. Allen, "Development of characterization tools for reliability testing of MicroElectroMechanical system actuators," *Proc. of SPIE*, **Vol. 3880**, 1999, pp. 156-164.

[18] S. T. Patton, W. D. Cowna, K. C. Eapen, and J. S. Zabinski, "Effect of surface chemistry on the tribological performance of a MEMS electrostatic lateral output motor," *Tribology Letters*, **Vol. 9**, No. 3-4, 2000, pp. 199-209.

[19] U. Srinivasan, J. D. Foster, U. Habib, R. T. Howe, R. Maboudian, S. C. Senft, and M. T. Dugger, "Lubrication of Polysilicon Micromechanisms with self-assembled Monolayers," *Proc. IEEE Solid-State Sensor Actuator Workshop*, Hilton Head, SC, USA, 1998, pp.156-161.

[20] Irwin L. Singer, "How Third-Body Processes Affect Friction and Wear," *MRS Bulletin*, **Vol. 23**, No. 6, June 1998.

[21] E. Rabinowicz, *Friction and Wear of Materials*, John Wiley & Sons, Inc., 1995, pp.143-190.

[22] M. Mosleh, N. Saka, and N. P. Suh, "A mechanism of high friction in dry sliding bearings," *Wear*, **252**, 2002, pp.1-8.

[23] E. Rabinowicz, *Friction and Wear of Materials*, John Wiley & Sons, Inc., 1995, p. 180.